Linking Physics-Based Deterioration Model to Field-Based Condition Assessments for Improving Asset Management

FINAL REPORT
January 2022

Submitted By:

Ravi Ranade
Associate Professor

Pinar Okumus
Associate Professor

University at Buffalo
212 Ketter Hall, Buffalo, NY 14260

External Project Manager:

John Picard, PE
Resident Engineer
LaBella Associates, Rochester NY
Former Regional Bridge Maintenance Engineer
New York State DOT - Region 5 (Buffalo)

In cooperation with

Rutgers, The State University of New Jersey
And
U.S. Department of Transportation
Federal Highway Administration

Disclaimer Statement

The contents of this report reflect the views of the authors, who are responsible for the facts and the accuracy of the information presented herein. This document is disseminated under the sponsorship of the Department of Transportation, University Transportation Centers Program, in the interest of information exchange. The U.S. Government assumes no liability for the contents or use thereof.

The Center for Advanced Infrastructure and Transportation (CAIT) is a Regional UTC Consortium led by Rutgers, The State University. Members of the consortium are Atlantic Cape Community College, Columbia University, Cornell University, New Jersey Institute of Technology, Polytechnic University of Puerto Rico, Princeton University, Rowan University, SUNY - Farmingdale State College, and SUNY - University at Buffalo. The Center is funded by the U.S. Department of

1. Report No.	2. Government Accession No.	3. Recipient's Catalog No.
CAIT-UTC-REG48		

4. Title and Subtitle	5. Report Date
Linking Physics-Based Deterioration Model to Field-Based Condition Assessments for Improving Asset Management	January 1, 2022
	6. Performing Organization Code CAIT/University at Buffalo
7. Author(s) Ravi Ranade https://orcid.org/0000-0001-6030-8371 Pinar Okumus https://orcid.org/0000-0002-2197-3261 Hanmin Wang https://orcid.org/0000-0001-5834-1930	8. Performing Organization Report No. CAIT-UTC-REG48
9. Performing Organization Name and Address University at Buffalo 212 Ketter Hall, Buffalo, NY 14260	10. Work Unit No.
	11. Contract or Grant No. 69A3551847102
12. Sponsoring Agency Name and Address Center for Advanced Infrastructure and Transportation Rutgers, The State University of New Jersey 100 Brett Road Piscataway, NJ 08854	13. Type of Report and Period Covered Final Report 2/1/2021-1/31/2022
	14. Sponsoring Agency Code

15. Supplementary Notes
U.S. Department of Transportation/OST-R
1200 New Jersey Avenue, SE
Washington, DC 20590-0001

16. Abstract

Currently used asset management programs by various state departments of transportation (DOT) rely typically on field-based condition assessments (periodic inspections and deterioration curves) of bridges for planning repair and maintenance activities. However, field inspections are labor intensive and can be subjective. Furthermore, visual inspections rely on visible signs of deterioration on the exterior surface of a bridge (e.g., corrosion stains and cracks) and may miss severe localized deterioration hidden inside concrete, which could incur significant repair costs in the future. On the other hand, physics-based models rely on simulating the underlying deterioration mechanisms for predicting future deterioration. Several parameters used in physics-based models are often based on extrapolating laboratory data that is not representative of field conditions. Furthermore, the outputs of physics-based deterioration model (e.g., rebar area loss) cannot be translated to condition ratings and are therefore unusable in asset management programs of state DOTs. For addressing these limitations, this research aims to (1) determine a rational basis for linking the outputs of a physics-based corrosion model to field-based condition ratings, and (2) calibration of input parameters of physics-based corrosion model based on deterioration curves obtained from field-based assessments. This report presents a systematic procedure for achieving these two aims. An example bridge column owned by New York State DOT is used to demonstrate the procedure. Links between the surface crack width and spalling and bridge element condition rating were established based on the interpretation of condition ratings. Inputs of the corrosion model were calibrated by matching the crack widths and spalling interpreted from deterioration curves with the outputs of the physics-based corrosion model. This project is expected to improve asset management by supplementing the field-based condition assessments with physics-based deterioration models.

17. Key Words	18. Distribution Statement
Condition rating; Deterioration; Corrosion rate; Cracking; Service life; Asset management	

19. Security Classification (of this report)	20. Security Classification (of this page)	21. No. of Pages	22. Price
Unclassified	Unclassified	47	

Acknowledgments

This research was financially supported by the Region 2 University Transportation Center, which is funded by the US Department of Transportation and by University at Buffalo (UB), the State University of New York. Financial support was also provided by the Institute of Bridge Engineering at UB. These financial supports are gratefully acknowledged. The opinions, findings and views expressed in this study are the ones of the authors only and do not necessarily reflect the views, policies, standard specifications or regulations of the parties acknowledged above. Funding agencies do not assume any liability for the contents or the use thereof.

Table of Contents

List of figures

List of tables

Nomenclature

A_0	Original rebar area
A_1	Area parameter 1 depending on D_0, $P(t)$, θ_1 and b in pitting corrosion model
A_2	Area parameter 2 depending on D_0, $P(t)$, θ_2 and b in pitting corrosion model
$A(t)$	Rebar area at time t
A_R	Ratio of exceedance frequency at a given PGA to the exceedance frequency at a PGA that is 10-times smaller than this PGA
b	Width of the pit area
C	Thickness of concrete cover
$C_{CI}(x,t)$	Chloride concentration at spatial coordinate x and time t
C_s	Chloride content at the outer surface of concrete
D_{CI}	Effective chloride diffusion coefficient
D_0	Original rebar diameter
d	The limiting value of EDP used to define a damage level
E	Elastic modulus of concrete
EDP	Engineering demand parameter
erf (.)	Error function
f_0	Yield strength of non-corroded reinforcement
$f(t)$	Yield strength of corroded rebar at time t
$f_t(t)$	Yield strength of transverse rebar at time t

f'_c	Compressive strength of unconfined concrete
$f_{cc}(t)$	Compressive strength of confined concrete at time t
IM_i	Ground motion intensity measure
$H(a)$	Probability of exceeding of a PGA (a)
K	The ratio of $\lambda(t)_{afcrack}$ to $\lambda(t)_{bfcrack}$
K_H	Slope parameter
M_{loss}	Mass loss of steel per unit length consumed to produce rust
M_r	Mass of rust per unit length of one rebar
m_{loss}	Percent of rebar mass loss (or area loss per unit length) due to corrosion
m	Number of ground motion intensity levels
n_j	Total ground motion records at j^{th} ground motion intensity levels
$P(t)$	Pit depth
P_{corr}	Internal pressure caused by rust expansion
Q_{corr}	Percent weight loss (or area loss) of rebar
R	Pitting factor
r_0	Radius of the thick-wall cylinder (concrete cover)
r_i	Radius of rebar
r	Distance from the center of the thick-wall model to the interface between the rust and concrete
T_1	Time when the peak corrosion rate is reached
t_{cr_lon}	Longitudinal rebar corrosion initiation time
$W(t)$	Crack width of concrete cover at time t
W_{cri}	Critical crack width

$W_{i,i=1,2,3}$	Fitting coefficients
z_j	Number of records which cause a particular damage state in the j[th] IM level
i_{corr}	Current density
β	Parameter of standard normal distribution
$\bar{\beta}$	Estimated parameter of standard normal distribution
δ_0	Thickness of the porous zone
δ_c	Radial displacement caused by rust expansion
ε_{cu}	The maximum compressive strain in the confined concrete
ε_{su}	Strain in transverse rebar at ultimate strength
θ	Parameter of standard normal distribution
$\bar{\theta}$	Estimated parameter of standard normal distribution
θ_1	Angle parameter 1 depending on D_0, $P(t)$, and b in pitting corrosion model
θ_2	Angle parameter 2 depending on D_0, $P(t)$, and b in pitting corrosion model
$\lambda(t)_{corr}$	Corrosion rate in mm/year
$\lambda(t)_{afcrack}$	Corrosion rate at critical crack width
$\lambda(t)_{bfcrack}$	Corrosion rate before cracking
ρ_{long}	Longitudinal reinforcement ratio
ρ_r	Mass density of rust
ρ_s	Mass density of the original (non-corroded) steel
$\rho_{trans}(t)$	Volumetric ratio of transverse rebar at time t

$\Delta A(t)$	Cross-sectional area loss of reinforcement at time t
$\Phi(.)$	Standard normal cumulative distribution function (CDF)
ν	Poisson's ratio of concrete
σ	Circumferential stress caused by rust expansion

Chapter 1. Introduction

The goal of infrastructure asset management is to preserve and manage the infrastructure sustainably, while ensuring safety and functionality during its service life [1, 2]. For reinforced concrete (RC) bridges, deterioration mechanisms such as corrosion can gradually affect safety and functionality. If left unaddressed, managing corrosion can be economically unsustainable. An effective asset management program must therefore be able to predict deterioration and optimize the timing of repair activities for maximizing safety and functionality under given budget and time constraints.

Field inspections are typically used to monitor the condition of bridges, and the resulting condition ratings are used as input in asset management tools and software for determining the repair priority of bridges, considering budget and time limitations. However, field inspections are labor intensive and can be subjective. Furthermore, visual inspections rely on visible signs of corrosion on the exterior surface of a bridge (e.g., corrosion stains and cracks), and may miss severe cases of localized deterioration until dangerously severe reinforcement corrosion occurs [3]. To address these challenges, a physics-based method is needed for supplementing field inspections improving the reliability of condition assessment and management of RC bridges.

Several researchers have developed models for estimating the condition of RC bridges using field-based condition assessments [4-6] or physics-based deterioration models [7-11]. Field-based condition assessment studies commonly develop deterioration models for bridges by collecting condition rating data from periodic bridge inspections and by processing this data using

deterministic or probabilistic regression/stochastic methods. These deterioration models are referred to as “deterioration curves”. Since corrosion is the main deterioration mechanism in RC bridges, studies based on physics-based deterioration models typically utilize corrosion models that are developed using fundamental equations of diffusion, supported by experimental data, and/or numerical simulations. The physics-based corrosion models estimate deterioration indicators, such as the rebar area loss, concrete crack width, concrete spalling, and the stiffness reduction of bridges as a function of time.

The existing studies [4-12] on condition assessment of RC bridges have several limitations or rely on several assumptions. Field-based condition ratings used to generate deterioration curves may have significant variability. This is partly due to the subjective nature of visual inspections [3]. Also, at a given bridge age, there is a wide scatter in the condition ratings due to large differences in the progression of deterioration in various bridges. These differences are caused by the unique characteristics of bridges in terms of their location, environmental exposure, traffic, etc. Therefore, the resulting average deterioration curve can be significantly different from the actual condition rating of an individual bridge at a given bridge age.

The physics-based models require input parameters, such as corrosion rate, relation between crack width and corrosion rate, which are difficult to measure in the field. These models estimate bridge deterioration in terms of indicators such as reinforcement area loss, concrete crack width, and concrete spalling as a function of time. However, the asset management systems used by various state departments of transportation (DOT) in the US rely on condition ratings from field inspections. A quantitative link between the indicators from the physics-based corrosion model

and the field condition ratings is missing. Such a link is needed for an objective assessment of structural health and for prioritizing maintenance and repair actions, given limited resources.

A systematic method linking the physics-based corrosion model to bridge condition ratings is proposed in this report to address some of the aforementioned limitations of existing models. The method consists of two parts: 1) a corrosion model, and 2) linking the corrosion indicators to bridge condition ratings. In the subsequent chapters of this report, an extension of the corrosion model introduced in Wang et al. [13] to capture spalling is presented. This extension is needed as spalling is used as a criterion in bridge condition rating. Next, bridge condition rating systems and deterioration curves currently used by transportation agencies are reviewed. Then, the method to link the corrosion model output (crack width and spalling) to the bridge deterioration curves is introduced. The application of the method is demonstrated using an example bridge. Finally, a parametric study is presented to identify the influence of critical parameters on the proposed method.

Chapter 2. Corrosion modeling for predicting concrete spalling

The methods for estimating the corrosion initiation time as well as modeling crack width as a function of time and corrosion rate are given in Wang et al. [13]. The focus of this chapter is to extend the corrosion model discussed in Wang et al. [13] to predict concrete spalling as concrete spalling is considered in condition rating of bridges.

2.1 Simplified concrete spalling geometry

Many studies [14-16] assumed a simplified triangular concrete spalling area on a cross-section view as shown in Figure 1. In this triangular spalling model, three cracks are assumed to form in the concrete cover. The angle between one of the outside cracks and the exterior surface of concrete cover is denoted by $\theta_{spalling}$.

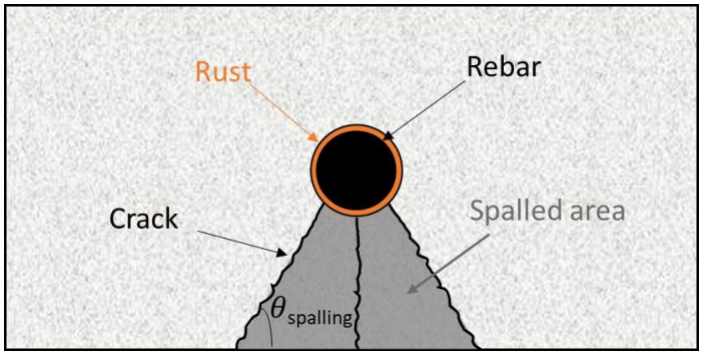

Figure 1: Simplified concrete spalling model shown in cross-section view

2.2 Pressure for concrete spalling

Moccia et al. [15] performed several experiments to investigate the relationship between the internal pressure caused by rust expansion and concrete spalling. In their experiments, a hydraulic device was inserted into a circular hole created in a concrete sample to apply radial pressure, simulating rust expansion. When concrete spalling was observed during the test, the corresponding pressure was recorded. By analyzing the test data and following a simplified model, a semi-empirical model considering the tensile strength of concrete, cover thickness and rebar size was developed to calculate the pressure for concrete spalling. The spalling pressure is calculated by Equation (1) using this model:

$$p_{spalling} = \frac{\eta_{ct} \times f_{ct}}{\tan(\theta_{spalling})} \times 2\sqrt{\frac{c}{\emptyset_{rebar}} + \left(\frac{c}{\emptyset_{rebar}}\right)^2} \times \left(\frac{\emptyset_0 d_{dg}}{\emptyset_{rebar} d_{dg0}}\right)^{1/m_{size}} \quad (1)$$

In the above equation, η_{ct} is the factor to account for the concrete brittleness in tension, f_{ct} is the concrete tensile strength (MPa), $\emptyset_0$ is the reference rebar size which is 20 mm and d_{dg0} is the reference aggregate size which is 32 mm [15], $\emptyset_{rebar}$ is the rebar size (mm), d_{dg} is the average roughness (mm), which is related to the maximum aggregate size (mm), c is the concrete cover thickness (mm) and m is the empirical coefficient from regression. This semi-empirical study used Imperial Units.

As mentioned in Wang et al. [13], over time, the build-up of rust increases tensile stress in the concrete surrounding the rebar. When this stress reaches the tensile strength of concrete, a crack is formed in the concrete cover. Rebar mass loss is predicted by Equation (2) shown below (also defined in Wang et al. [13]). In this equation, m_{loss} is the percent rebar mass loss as a function

of time, and Q_{corr} is the percent area loss of rebar as a function of time. Lu et al. [17] proposed an equation for internal radial pressure (P_{corr}) due to rust expansion, given by Equation (3). This equation accounts for the fact that when rust layer becomes thick (between crack initiation time and time of concrete spalling), the rust layer will be restrained and compressed by the surrounding concrete [18, 19], and therefore, the deformation of the rust layer should be considered. In Equation (3), δ_0 is the thickness of the porous zone around the rebar, n is the volume expansion coefficient (due to greater volume of corrosion products compared to the reactants), $\emptyset_{rebar}$ is the rebar diameter, E_c is the elastic modulus of concrete, E_r is the elastic modulus of rust, v and ν_r are the Poisson's ratios of concrete and rust, respectively. Assuming that all the corrosion products remain inside, the internal radial pressure, corresponding to the rebar mass loss computed by Equation (2), can be found using Equation (3) [17].

$$m_{loss} = Q_{corr} \times unit\ thickness\ of\ section\ (1\ mm) \tag{2}$$

$$\begin{cases} P_{corr} = \dfrac{\sqrt{1+(n-1)m_{loss}/100}-1-2\delta_0/\emptyset_{rebar}}{\frac{1}{E_c}\left[\frac{(r_z+C)^2+r_z^2}{(r_z+C)^2-r_z^2}\right]+v-\frac{1}{E_r}\left[\frac{nm_{loss}/100(1-\nu_r^2)\sqrt{1+(n-1)m_{loss}/100}}{[(1+\nu_r)n-2](m_{loss}/100)+2}\right]} \\ where\ r_z = \dfrac{\emptyset_{rebar}}{2}+\delta_0 \end{cases} \tag{3}$$

The time at which concrete spalls is determined by checking whether the radial pressure due to rust expansion calculated by Equation (3) reaches the concrete spalling pressure determined by Equation (1). Later in this report, the concrete spalling pressure is calibrated by changing the parameter $\theta_{spalling}$ in Equation (1) as will be discussed in Chapter 6.

Chapter 3. Review of bridge inspection programs and condition ratings

The bridge inspection program in the US was established in 1968 in the aftermath of the collapse of the 2,235-foot Silver Bridge, at Point Pleasant, West Virginia. After the failure of the bridge, the USDOT decided to establish a national bridge inspection standard [20] to keep bridges safe and serviceable. After several decades of development, the bridge inspection program became more standardized, more sophisticated and broader in scope compared to the first version. For example, different procedures have been developed for different types of bridge inspections [21] and new inspection technologies have been developed, such as sonic testing and spectrum analysis [20]. One of the most common inspection types is routine inspection, which is a two-year periodic inspection during the service life of a bridge. Routine inspection uses measurements and observations to evaluate the condition of bridges and documents changes in condition since the last inspection.

Visual inspection (observations) is the primary method used in routine inspection. It is commonly performed by inspection teams consisting of several trained bridge inspection engineers. During each inspection, the inspection engineers examine all bridge components, such as bridge deck, girders, bearing, and bridge columns/bridge pier walls, and document the location, type, size, quantity, and description of damage severity such as area of concrete spalling and surface crack widths. The inspection engineers assign a number (0~7 or 0~9) to the examined bridge elements, which is called bridge element condition rating. Similarly, bridge component ratings are used to evaluate the overall condition of the superstructure and substructure of a bridge. The method

presented in this report uses bridge element condition rating data. Additional details about the rating systems can be found in the AASHTO Manual for Bridge Inspection [21].

The New York Department of Transportation (NYSDOT) used two different rating systems. Before 2016, NYSDOT's bridge inspection system had a scale of 1 (failure) to 7 (new) to evaluate the condition of a bridge component. The description of each condition rating is given in Table 1. After 2016, NYSDOT transitioned to AASHTO's element-based condition rating system (AASHTO ECR). This system has rating scales ranging from CS1-good to CS4-severe, following AASHTO Manual for Bridge Inspection [21]. Table 2 shows the AASHTO ECR guidelines. The method presented in this report utilizes both scales due to their unique advantages. AASHTO ECR scale (CS1 to CS4) is used because it provides more detailed information on elements. However, since this system is newer (since 2016), data collected using this scale are limited to a relatively short period. The older NYSDOT scale (1 to 7) is less detailed but have been used over a longer period leading to a larger condition rating data set.

Table 1: Condition rating guidelines of NYSDOT bridge component evaluation (adapted from NYSDOT [22])

Condition rating	Description
7	New condition, no deterioration.
6	Used to shade between rating s of 5 and 7.
5	Minor deterioration, but functioning as originally designed.
4	Used to shade between ratings of 3 and 5.
3	Serious deterioration, or not functioning as originally designed.
2	Used to shade between ratings of 1 and 3.
1	Totally deteriorated, or in failed condition.

Table 2: AASHTO ECR guidelines (adapted from NYSDOT [23])

Condition State	Condition Type	General Condition Guideline
CS-1	Good	That portion of the element that has either no deterioration or the deterioration is insignificant to the management of the element, meaning that portion of the element has no condition based preventive maintenance needs or repairs. Areas of an element that have received long lasting structural repairs that restore the full capacity of the element with an expected life equal to the original element may be coded as good condition.
CS-2	Fair	That portion of the element that has minor deficiencies that signify a progression of the deterioration process. This portion of the element may need condition based preventive maintenance. Areas of the element that have received repairs that improve the element, but the repair is not considered equal to the original member may be coded as fair.
CS-3	Poor	That portion of the element that has advanced deterioration but does not warrant structural review. This portion of the element may need condition based preventative maintenance or other remedial action.
CS-4	Severe	That portion of the element that warrants a structural review to determine the effect on strength or serviceability of the element or bridge; OR a structural review has been completed and the defects impact strength or serviceability of the element or bridge; OR a condition where that portion of the element is no longer effective for its intended purpose.
CS-5	Unknown	That portion of the element not assessable due to lack of access.

Chapter 4. Review of bridge deterioration curves

Bridge element deterioration curves are developed using historical element condition rating data of many bridges in a certain region. These curves are used to estimate the future condition of bridges in the region and to plan intervening actions. Because the curves are developed based on inventory data, deterioration curves represent average performance of bridges in the inventory rather than the performance of individual bridges.

As mentioned in Chapter 1, deterioration curves are commonly developed by two methods: deterministic methods and stochastic methods. Deterministic methods [5, 24, 25] utilize statistical regression for determining the relationship between the bridge condition rating and time. The deterministic deterioration curves can be developed using straight-line, extrapolation, regression, and curve-fitting methods [5].

The stochastic methods [4, 5, 26] capture the uncertainty and randomness in bridge deterioration. The models developed by stochastic methods can be classified as either state-based or time-based [26]. In state-based models, deterioration models are commonly modeled by Markov chains, which represent the change of bridge condition ratings within a certain time (e.g., 2 years between successive inspections) as a probability matrix. The probability matrix can be developed using the bridge condition rating data and optimization theories. Then, the relationship between the estimated bridge condition rating and time can be developed based on the probability matrix. In time-based models, the duration of a bridge component at a particular bridge condition rating is modeled as a random variable using either a Weibull-based probability distribution or a lognormal

distribution. The probability distribution is developed by fitting the time-based model with the bridge condition rating data.

Chapter 5. Deterioration interpretation from bridge element condition ratings

The goal of this report is to establish a link between the physics-based corrosion indicators (e.g., crack width) and the field-based bridge element condition ratings. In this chapter, the bridge element condition ratings are correlated with crack width and spalled area, which are later used as the basis of the linkage to the physics-based indicators. For this purpose, two relationships are needed: (1) the relationship between the corrosion indicators and the AASHTO ECR, and (2) the relationship between the AASHTO ECR and the NYSDOT element condition ratings (NYSDOT ECR). It should be noted that element condition ratings from other states can also be used for this practice. NYSDOT ECR are used in this study because of their availability to the author.

To establish the first relationship mentioned above, Table 3 presents a correlation between crack widths and condition ratings of RC bridge columns, as described in AASHTO ECR [21]. Similarly, using the same reference [21], Table 4 presents a correlation between area of concrete spalling and condition ratings of RC bridge columns. In this study, crack width and concrete spalling are used as corrosion indicators.

Table 3: Condition states of reinforced concrete elements based on surface crack widths (adapted from AASHTO [21])

Condition State	Defect	Description
CS-1	Insignificant cracks or moderate width cracks that have been sealed	Cracks less than 0.012''(0.3 mm) in width can be considered "insignificant" and a defect is not warranted under the Element.
CS-2	Unsealed moderate width cracks or unsealed moderate pattern (map) cracking.	Cracks ranging from 0.012''(0.3 mm) up to 0.05'' (1.27 mm) can be considered "moderate" .
CS-3	Wide crack or heavy pattern (map) cracking.	Cracks equal to or greater than 0.05''(1.27 mm) can be considered "wide". Extent and severity are not excessive and/or widespread,
CS-4	Wide crack or heavy pattern (map) cracking including ASR.	The condition is beyond the limits established in condition state three (3) and /or warrants a structural review to determine the strength or serviceability of the element or bridge.

Table 4: Condition states of reinforced concrete elements based on areas of concrete spalling (adapted from AASHTO [21])

Defect	CS-1 - Good	CS-2 - Fair	CS-3 - Poor	CS-4 - Severe
Delamination /Spall	None	Spall less than 1 inch (25 mm) deep or less than 6 inches in diameter	Spall greater than 1 inch (25 mm) deep or greater than 6 inches (152.4 mm) in diameter or exposed rebar	The condition is beyond the limits established in condition state three (3) and /or warrants a structural review to determine the strength or serviceability of the element or bridge.

The second relationship mentioned above, between the AASHTO ECR and the NYSDOT ECR, is needed because (1) the AASHTO ECR system has been effective in New York State only after 2016. Therefore, there is limited historical data for developing deterioration curves using AASHTO ECR, and (2) existing deterioration curves in the literature for bridge elements in New

York State are generated based on the NYSDOT ECR, but the relationships between NYSDOT ECR and crack width are not well-quantified.

The relationship between AASHTO ECR (CS-1 to CS-5) and NYSDOT ECR (1 to 7) is established based on several assumptions and is shown in Table 5. AASHTO ECR of CS-4 is assumed to correspond to a NYSDOT ECR of 3 because they are both used to indicate loss of functionality of a bridge element. AASHTO ECR of CS-2 is assumed to correspond to a NYSDOT ECR of 5 because both represent minor deterioration in a bridge element. AASHTO RCR of CS-1 is assumed to correspond to the NYSDOT ECR of 7 and 6 because both are assigned to elements with no deterioration or insignificant deterioration. Based on the aforementioned definitions, the remaining AASHTO ECR of CS-3 is assumed to correspond to NYSDOT ECR of 4. The condition states CS-4 and CS-3 have no differences in terms of crack width (see Table 3). Therefore, only CS-3 was considered in the relationship between AASHTO ECR and NYSDOT ECR.

Due to the simplified model used in this study (Chapter 2.1), after concrete spalling, the depth of the spalled area is assumed to be equal to the thickness of the concrete cover. For most concrete transportation structures, the cover thickness is at least 1 inch. Therefore, when the time for concrete spalling is reached, the condition rating is assumed to drop down to CS-3.

Using the two relationships described above (between crack width/spalling and AASHTO ECR, and between AASHTO ECR and NYSDOT ECR), NYSDOT ECR is defined in terms of crack width and concrete spalled area as shown in Table 5. It should be noted that the assumptions made to connect the AASHTO ECR to NYSDOT ECR can be modified and refined in the future,

but these assumptions do not change the procedures for the general method of linking physics-based and field-based methods described in the subsequent chapters.

Table 5: Relationship between NYSDOT ECR and crack width

NYSDOT bridge element condition rating	**7**	**6**	**5**	**4**
AASHTO bridge element condition rating	CS-1	CS-1	CS-2	CS-3
Crack width (W), inch	$W = 0$	$0 < W \leq 0.012$	$0.012 < W \leq 0.05$	$W > 0.05$
Spalled area	N/A	N/A	Spall less than 1 inch deep or less than 6 inch diameter*	Spall greater than 1 inch deep or greater than 6 inch diameter*

* Since the depth of the spalled area is assumed to be the cover thickness and since cover thickness is larger than 1 inch for most bridges, spalling is assumed at NYSDOT ECR of 4 or AASHTO ECR of CS-3.

Chapter 6. Corrosion model calibration

The corrosion model parameters, corrosion rate ($\lambda(t)_{bfcrack}$), pitting factor (R), corrosion initiation time, the ratio (K) of $\lambda(t)_{afcrack}$ to $\lambda(t)_{bfcrack}$ and critical crack width (W_{cri}), can be calibrated using the deterioration curves introduced in Chapter 4. These curves represent the average deterioration rate of bridges in a state or a region. Although the bridge inspection data of a particular bridge can also be used for calibration, this data is limited, especially for bridges built within the last 10 years. Using a limited data set to calibrate the corrosion model would cause a large bias. Moreover, bridge deterioration curves are the most commonly used tools by state DOTs for asset management. Therefore, using these curves for model calibration is relevant and is expected to accelerate adoption by practicing engineers.

The method for calibrating the inputs of the corrosion model is illustrated in Figure 2 and Figure 3. In the first calibration step, crack width is used as the criterion for calibration. The corrosion model calculates the crack width as a function of bridge age (Wang et al. [13]). Deterioration curves provide the bridge ECR as a function of bridge age, but they can be converted to equivalent crack widths as a function of bridge age using the interpretation described in Table 5. The output of this step is the lower and upper bounds of crack widths and average of the bounds corresponding to a condition rating. The calibration process involves using the least sum of squares method to minimize the difference between crack width calculated by the corrosion model ($W(t_i)$) and the average crack width ($W_{ave}(t_i)$) calculated as the average of the upper ($W_{UB}(t_i)$) and lower bound ($W_{LB}(t_i)$) of crack widths derived from the deterioration curves as shown in Equation (4a). If the crack width range determined from the deterioration curves does not have an upper bound value (e.g., crack width > 0.05 inch for NYSDOT ECR of 4 and AASHTO ECR of

CS-3 in Table 5), the crack width calculated by the corrosion model should be larger than the lower bound crack width determined from the deterioration curves (Equation (4b). The inputs of the corrosion model, such as $\lambda(t)_{bfcrack}$, are changed iteratively until the conditions given in Equation (4) are satisfied.

$$\left.\begin{array}{l} (a)\ W_{ave}(t_i) = \frac{W_{UB}(t_i)+W_{LB}(t_i)}{2} \\ (b)\ if\ W_{UB}(t_i)\ is\ defined, \sum_{i=1}^{N=2}[W(t_i) - W_{ave}(t_i)]^2 \cong 0 \\ (c)\ if\ W_{UB}(t_i)\ is\ not\ defined, W(t) \geq W_{LB}(t) \end{array}\right\} \quad (4)$$

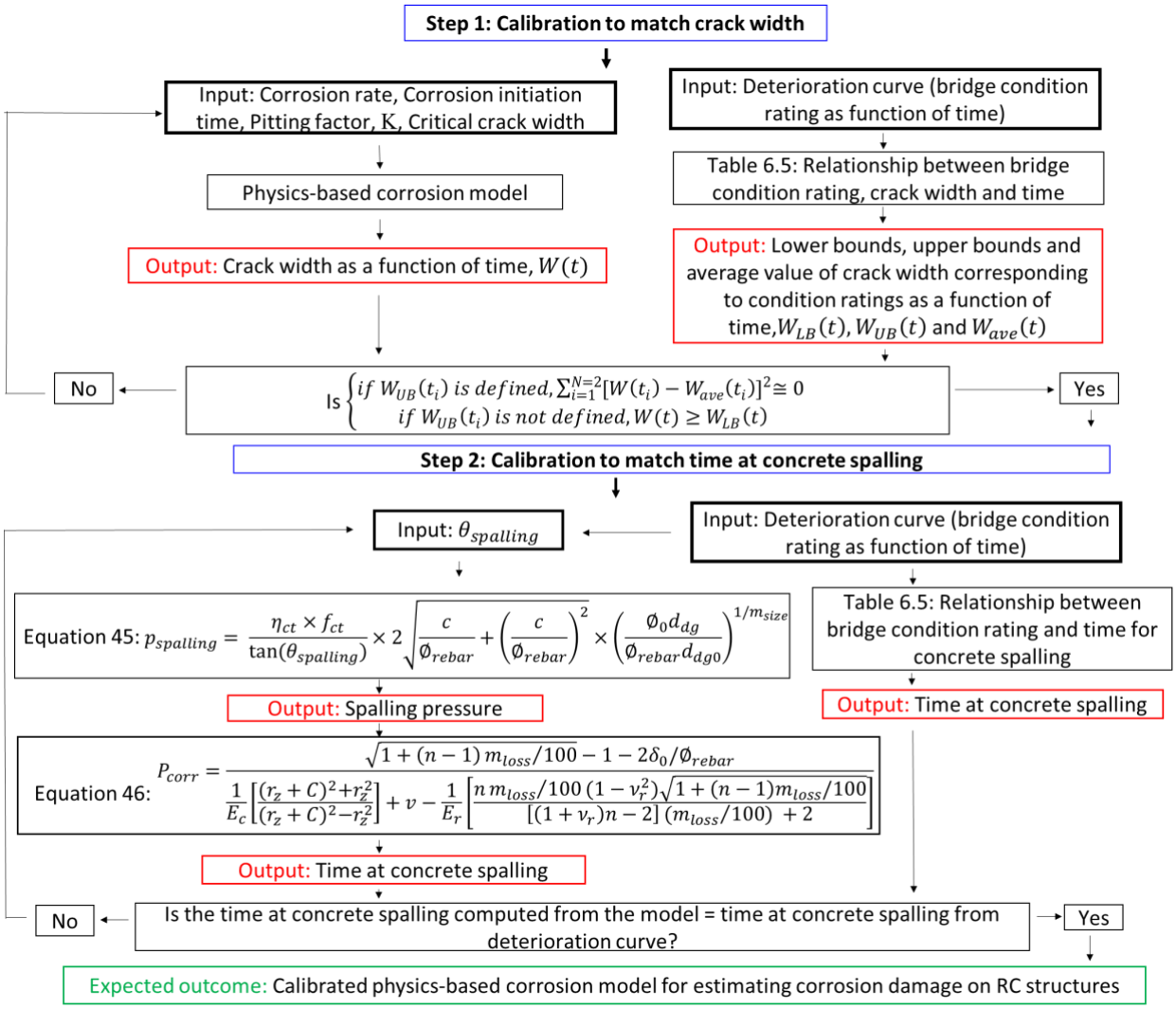

Figure 2: Calibration framework

In the second calibration step, concrete spalling criterion is checked by iteratively changing the cracking angle $\theta_{spalling}$. Physically, the cracking angle is governed by the aggregate size, aggregate location, and the aggregate-cement paste interfacial characteristics. Due to the complexity of the concrete spalling process, it is difficult to accurately estimate $\theta_{spalling}$ from fundamental parameters. Therefore, this variable was calibrated using field-data. In this study, $\theta_{spalling}$ in Equation (1) is calibrated in the range of 15° to 75° [14, 16] to ensure that the criteria

shown in Table 5 for both crack width and spalling are satisfied simultaneously. Figure 3 demonstrates the process of calibration.

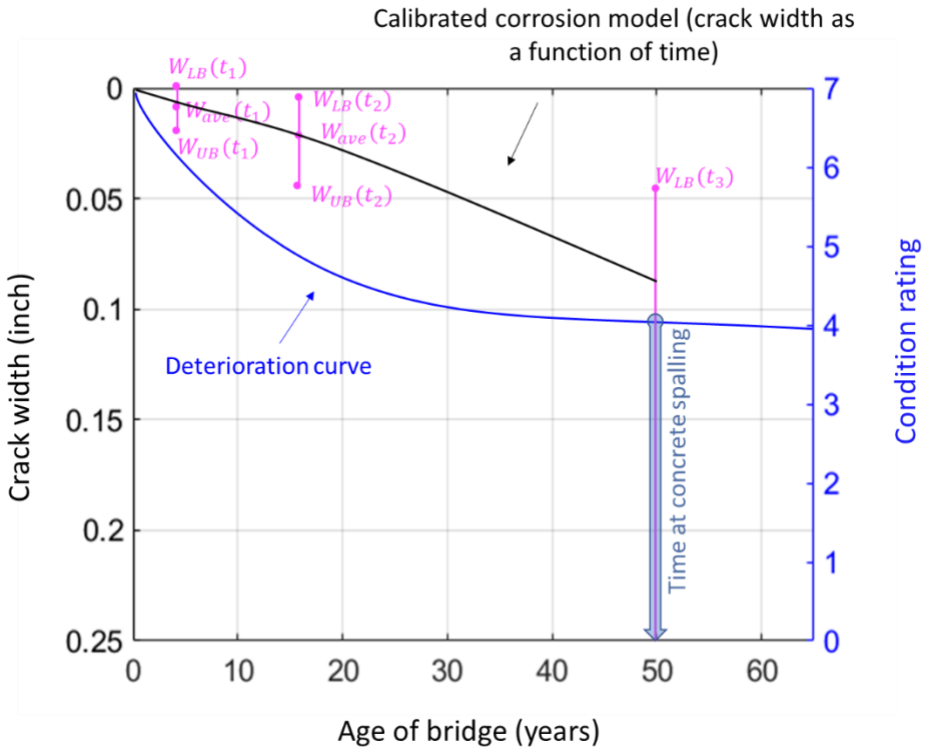

Figure 3: Demonstration of the calibration process

Chapter 7. Demonstration of the calibration process with an example

An example RC bridge located in Erie County, NY, crossing over a 2-lane state route, is used to demonstrate the calibration process. The bridge has two spans and a concrete deck supported by two RC bridge columns, exposed to a large amount of deicing salts during the winter season. In this study, the corrosion rate of one bridge column was calibrated based on the deterioration curves. The deterioration curves used in this study were developed by Agrawal et al. [4], which represent the deterioration of concrete bridge columns in New York State. The deterioration function is expressed as shown in Equation (5), where T is the time in years since bridge construction. By using Equation (5) and Table 5, the criteria for the corrosion rate calibration can be developed as shown in Figure 4. It should be noted that the specific deterioration curve shown in Equation (5) appears as a "straight line" in Figure 4. Typically, the rate of deterioration (or decrease in condition ratings) reduces with time.

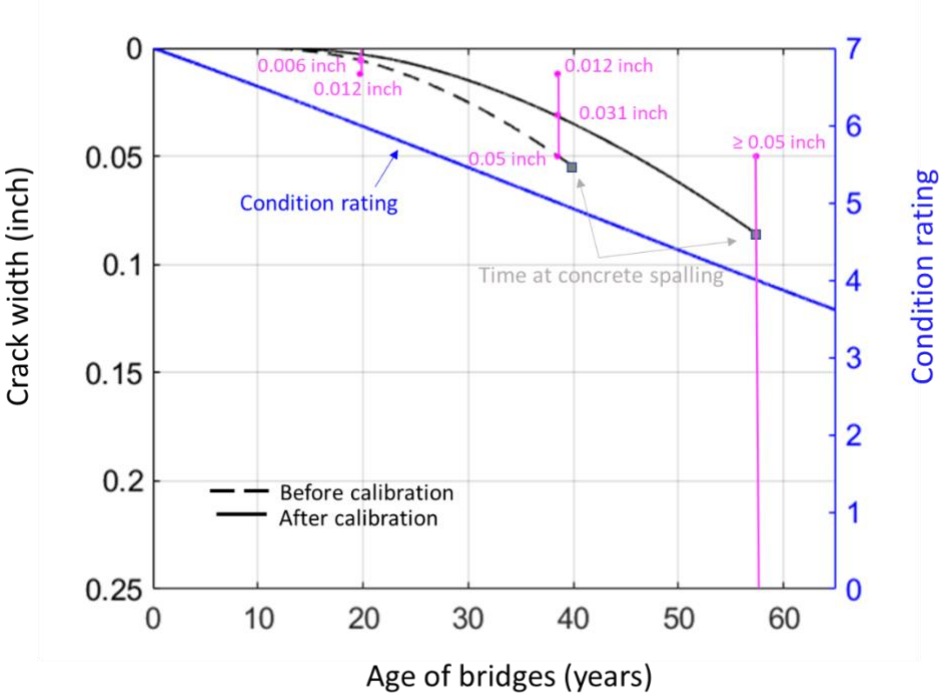

Figure 4: Calibration of corrosion rate before cracking ($\lambda(t)_{bfcrack}$)

In Figure 4, the blue line is the condition rating expressed by Equation (5). The pink lines were developed from the deterioration curve. They indicate the upper, lower bounds and average of crack width at a given condition rating and the time when concrete spalls based on the condition rating. The crack width ($W(t)$) curve computed by the corrosion model (the black line in Figure 6.4) should satisfy Equation (4).

$$NYSDOT\ ECR = 7 - 0.0486218T - 0.0001326T^2 + 0.0000012T^3 \qquad (5)$$

Before calibration, the corrosion initiation time of the bridge column is calculated by inputting the parameters shown in Table 6 into Equation (1) of Wang et al. [13]. These input parameters are within reasonable range, as supported by the references provided in Table 6. The corrosion initiation time is calculated as 3.3 years using this input. Wang et al. [13] showed that the corrosion rate before cracking ($\lambda(t)_{bfcrack}$) has the most significant effect on the corrosion model results. Therefore, the calibration of this parameter is presented in this example. The effects of calibrating other corrosion model inputs are discussed in Chapter 8.

Table 6: Model parameters of the bridge column

Corrosion model parameters	**Units**	**Values before calibration**	**Source**
C_s	lbs/yard^3	0.062	Weyers, Fitch [27]
D_{CI}	inch^2/year	0.13	Weyers, Fitch [27]
Critical chloride content at rebar surface	lbs/yard^3	2.02	Life-365™ [28]
Corrosion initiation time	years	3.3	-
C	inch	1.4	-
E_c	ksi	3704	-
$\lambda(t)_{bfcrack}$	inch/year	4.0×10^{-4} (before calibration)	Andrade and Alonso [29]
K	-	2	-
Critical crack width, (W_{cri})	inch	0.008	Cui, Zhang [30]
R	-	6	Val and Melchers [7]
E_r	ksi	3	Liu and Su [19]
ν_c	-	0.18	El Maaddawy and Soudki [31]
ν_r	-	0.5	Lu, Jin [17]
n	-	4	Lu, Jin [17], Liu and Su [19]
$\theta_{spalling}$	-	35° (before calibration)	Su and Zhang [16]

The procedure for calibrating the corrosion model for the example bridge is as follows:

Step 1: By inputting the value of $\lambda(t)_{bfcrack}$,W_{cri}, R, K and E_c in the corrosion model as illustrated in this and Wang et al. [13], the crack width as a function of time and time for concrete spalling is calculated (dashed line in Figure 4).

Step 2: The lower bound, upper bound and average of lower and upper bounds of crack width (pink dots) corresponding to bridge ages at which condition ratings (blue line) change are obtained from deterioration curves. At t_1= 19.7 years, $W_{LB}(t_1) = 0$ inches, $W_{UB}(t_1) = 0.012$ inches and $W_{ave}(t_1) = 0.006$ inches. At t_2= 38.5 years $W_{LB}(t_2) = 0.012$ inches, $W_{UB}(t_2) =$ 0.05 inches and $W_{ave}(t_2) = 0.031$inches. At t_3= 57.4 years, $W_{LB}(t_3) = 0.05$ inches.

Step 3: The crack widths calculated by the corrosion model (**Step 1**) are checked to determine whether they satisfy the conditions of Equation (4). If they do not, the corrosion rate ($\lambda(t)_{bfcrack}$) is changed and Step 1 is repeated iteratively until the conditions of Equation (4) are satisfied. For this example bridge, $\lambda(t)_{bfcrack}$ that satisfied the conditions given in Equation (4) was 3.8×10^{-4} inch/year.

The comparison between the predicted crack width before and after calibration is presented in Figure 4. The blue line is the deterioration curve developed by Agrawal et al. [4] for NYSDOT bridges. As shown in the figure, the calibrated value of $\lambda(t)_{bfcrack}$ is 3.8×10^{-4} inch/year. Before calibration, $\lambda(t)_{bfcrack}$ was 4.0×10^{-4} inch/year. The value before calibration resulted in crack

widths within the range of crack widths obtained based on the deterioration curve but closer to the upper bound crack width.

Step 4: Using E_r, υ_r, n, and υ_c shown in Table 6, the pressure due to rust expansion (Equation (3)) is calculated as a function of time. Before calibration, concrete spalled at 38 years, when the condition rating drops to NYSDOT ECR of 4, based on the assumption in Chapter 5. The parameter $\theta_{spalling}$ is calibrated iteratively until the concrete spalling criterion shown in Figure 4 is satisfied. The value of $\theta_{spalling}$ thus obtained from calibration is 33.5°.

Chapter 8. Effects of different corrosion input parameters on crack width

This chapter serves two purposes: (1) to identify input parameters that have negligible effects on the results so that calibration efficiency can be improved by excluding these parameters from the calibration process, (2) to identify the input parameter combinations that lead to a match between the corrosion model results and field-data.

In this chapter, the effects of different corrosion input parameters of the corrosion model were investigated by varying these parameters one at a time. The input parameters varied were the corrosion rate before cracking ($\lambda(t)_{bfcrack}$), pitting factor (R), the ratio (K) of $\lambda(t)_{afcrack}$ to $\lambda(t)_{bfcrack}$, corrosion initiation time, and critical crack width (W_{cri}). The example bridge presented in Chapter 7 was used as a baseline for this exercise. The values of the input parameters that led to a match between corrosion model and field-based data are summarized in Table 7 and discussed in this chapter.

Table 7: Values of the corrosion model input parameters that led to a reasonable match with field-based data

Corrosion model parameters	Units	Values	Typical range	Source for typical range
$\lambda(t)_{bfcrack}$	inch/year	2.9×10^{-4}, 3.3×10^{-4}, 3.8×10^{-4}*, 4.0×10^{-4}	2.0×10^{-4} ~ 4.0×10^{-4}	Andrade and Alonso [29]
R	-	4.8, 6.0*,7.3	4.0 ~ 8.0	Val and Melchers [7]
K	-	1.4, 2.0*, 2.6	-	-
Corrosion initiation time	years	3.3*, 5.0, 6.0, 7.0	-	-
Critical crack width, (W_{cri})	inch	0.004, 0.008*, 0.012	-	-

* Baseline values that were kept constant when other parameters changed one at a time.

Figure 5 shows that the crack width increases with an increase in $\lambda(t)_{bfcrack}$. This is because $\lambda(t)_{bfcrack}$ is the major factor determining the rebar area loss as shown in Wang et al. [13], which in turn influences the crack width. For the baseline values of R, K, corrosion initiation time, and critical crack width shown in Table 7, the minimum and maximum values that $\lambda(t)_{bfcrack}$ can take while keeping the predicted crack width within the range determined from deterioration curves are 2.9×10^{-4} inch/year and 4.0×10^{-4} inch/year, respectively, which are within the range reported by Andrade and Alonso [29].

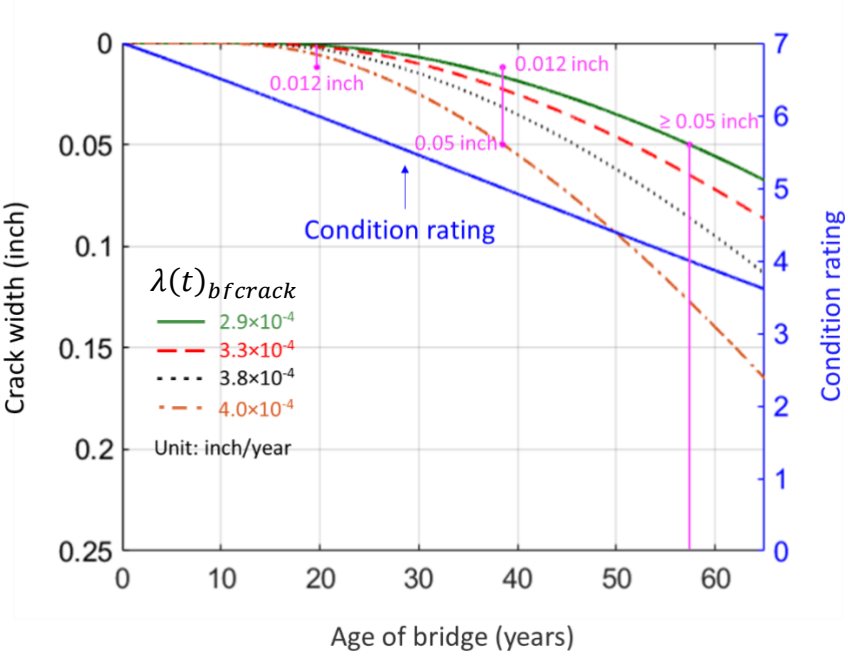

Figure 5: Effect of varying $\lambda(t)_{bfcrack}$ on crack width evolution

Figure 6 and Figure 7 show that the effect of the parameters R and K, respectively, on crack width are significant. This is attributed to the fact that, similar to $\lambda(t)_{bfcrack}$, R and K are major factors determining the rebar area loss in Equation (7). The minimum and maximum values of R that maintain the crack width consistent with those determined from deterioration curves are 4.8

and 7.3, respectively, when other parameters are assigned the baseline values shown in Table 7. The minimum and maximum values of K that are within the calibration range are 1.4 and 2.6, respectively, when other parameters are assigned the baseline values.

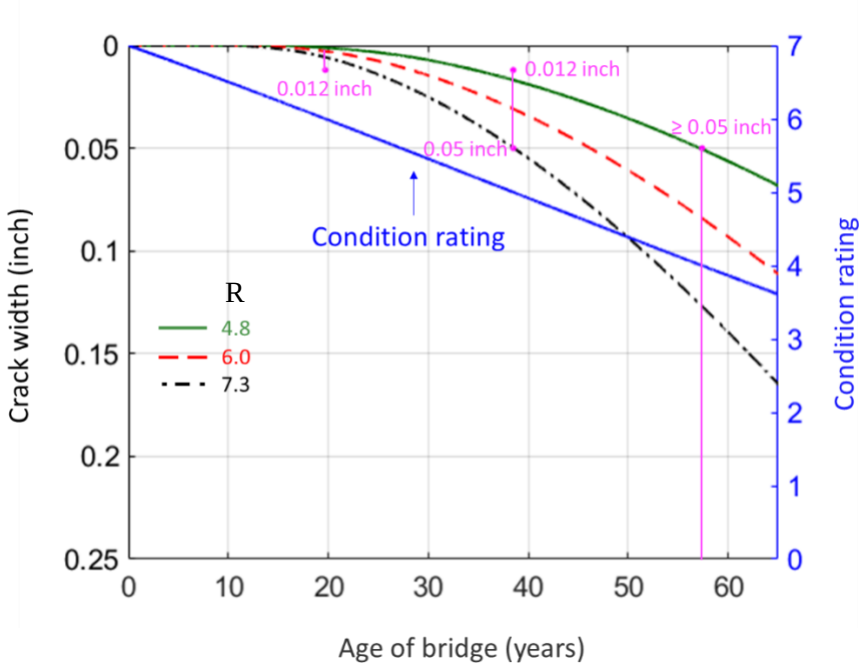

Figure 6: Effect of varying R on crack width evolution

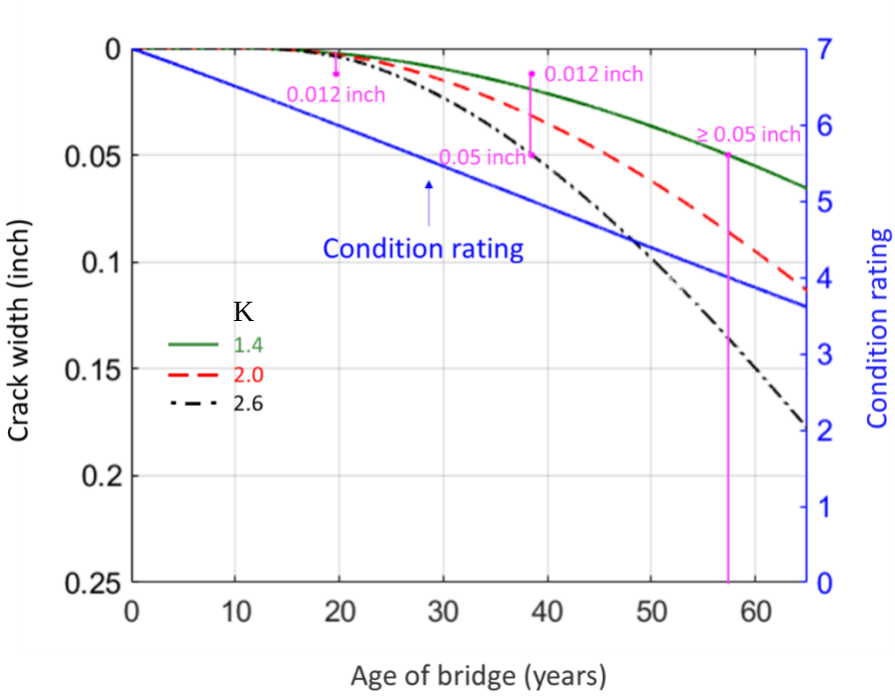

Figure 7: Effect of varying K on crack width evolution

Figure 8 shows that corrosion initiation time has negligible effects on crack width. This is likely because the corrosion initiation times (3 to 9 years) were small compared to the time scale considered (tens of years), which resulted in insignificant effects on the reinforcement area loss. It should be noted that $\lambda(t)_{bfcrack}$ also covers a short period before cracking (6-9 years). However, $\lambda(t)_{bfcrack}$ also influences the corrosion rate after cracking and the maximum corrosion rate and has a significant effect on the crack width. All reasonable values of corrosion initiation time led to crack widths that were within the calibration range, when other parameters were the baseline values shown in Table 7.

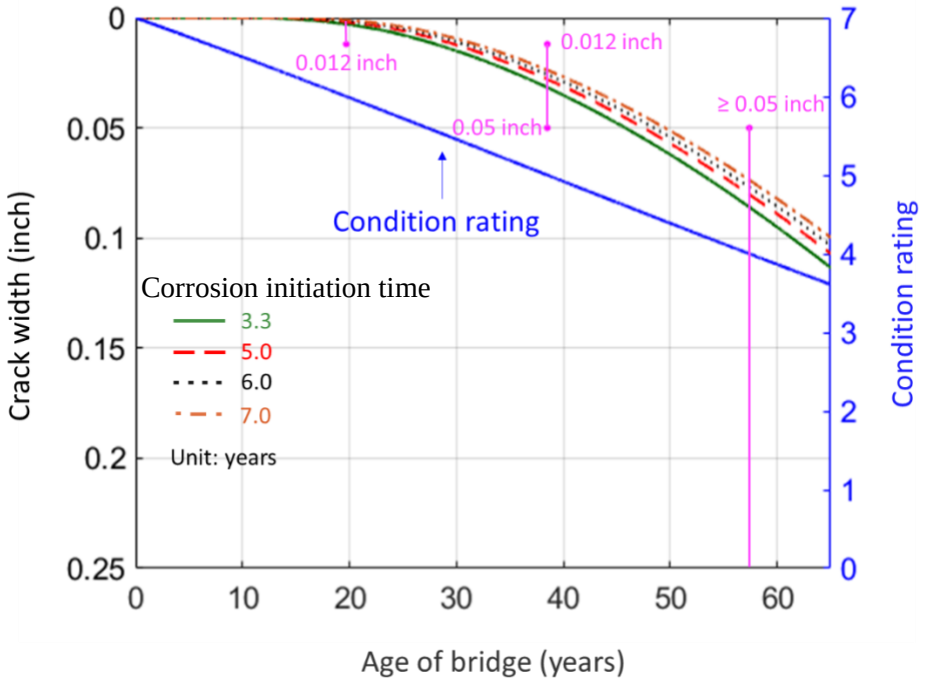

Figure 8: Effect of corrosion initiation time on crack width evolution

Figure 9 shows that crack width is not sensitive to W_{cri}, i.e., the critical crack width at which the corrosion rate reaches the maximum value. For the same $\lambda(t)_{bfcrack}$, R, and corrosion initiation time, the time at which concrete cracks computed by the corrosion model is the same. Therefore, W_{cri} only affects the time during which the corrosion rate increases, which is small (less than 10 years) compared to the service life of the bridges (75 years). Therefore, W_{cri} has a limited effect on crack width. When all other parameters are assigned the baseline values shown in Table 7, all reasonable values of W_{cri} lead to crack widths that are within the range determined from the deterioration curves.

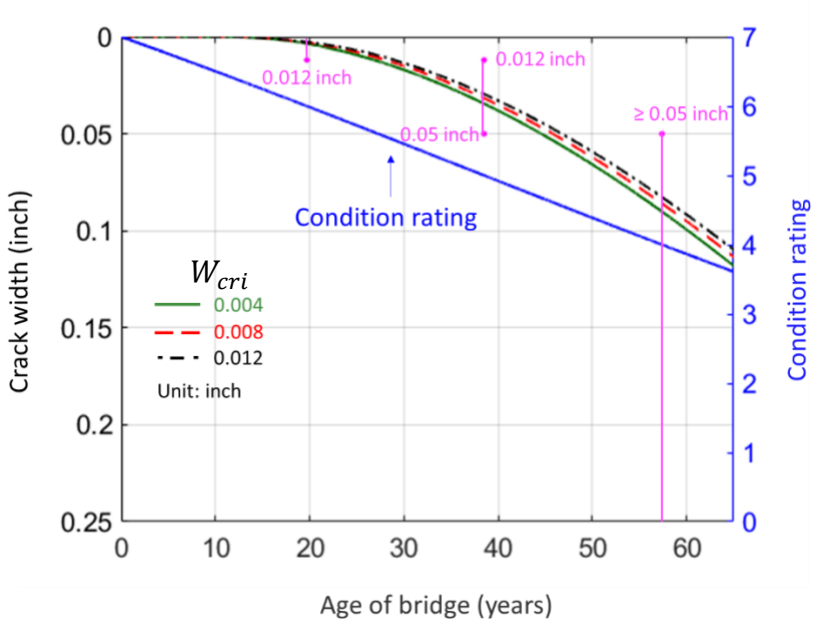

Figure 9: Effect of W_{cri} on crack width evolution

Based on the above results, the corrosion initiation time and W_{cri} do not need to be considered as parameters to be calibrated. Although the effects of R and K are significant, it is hard to collect data from real bridges or laboratory experiments for determining the values of these empirical parameters. In the literature (discussed in Wang et al. [13]), R ranges from 4 to 8 ([7]. It quantifies the distribution of pitting locations along a corroded rebar [11]. In real practice, it is difficult to observe all the corroded locations of a rebar embedded in a bridge column. For K, which is the ratio of corrosion rate after cracking to that before cracking, there are limited laboratory tests [32, 33] and no field observations. Thus, the most suitable parameter for calibration is determined to be the corrosion rate before cracking ($\lambda(t)_{bfcrack}$). $\lambda(t)_{bfcrack}$ determined from the calibration is within the range reported by Andrade and Alonso [29].

Chapter 9. Summary and conclusions

A systematic method for linking the physics-based corrosion model and the field-based condition assessments is proposed in this report. In this method, the physics-based corrosion model introduced in Wang et al. [13] was expanded by incorporating concrete spalling because spalling affects bridge condition ratings. Then, links between the surface crack width and bridge element condition rating, as well as concrete spalling and bridge element condition rating were established based on the guidelines of NYSDOT [23] and AASHTO [21]. Finally, based on the developed link, a calibration method for the inputs of the corrosion model was proposed by matching the crack widths and spalling interpreted from deterioration curves with the outputs of the physics-based corrosion model.

The use of the calibration method was demonstrated on an example bridge in New York State. The calibration identified a range for corrosion rates before cracking that leads to a match between the corrosion model and deterioration curve predictions. The upper bound of this range corresponded to the rate reported in the literature by others [29].

The effects of various model parameters, including the corrosion rate before cracking ($\lambda(t)_{bfcrack}$), pitting factor (R), the ratio (K) of $\lambda(t)_{afcrack}$ to $\lambda(t)_{bfcrack}$, corrosion initiation time and critical crack width (W_{cri}), were investigated. The results show that crack width increases with the increase of $\lambda(t)_{bfcrack}$, R, and K. Corrosion initiation time and W_{cri} have negligible effects on the crack width. $\lambda(t)_{bfcrack}$ is recommended as the most appropriate parameter to be calibrated in the proposed method because it is easier to be measured in real practice than other

parameters and has a significant effect on the crack width. $\lambda(t)_{bfcrack}$ determined from the proposed method is within the range reported by Andrade and Alonso [29].

DOTs can use the method presented in this report to calibrate the physics-based corrosion model for their bridge inventories and existing deterioration curves. The calibrated corrosion model can then be used to predict the future condition of bridges to inform decisions and prioritize actions for maintenance, repair and replacement. As such, the corrosion prediction model and its calibration procedure can support bridge management programs of DOTs.

References

1. AASHTO, *AASHTO Transportation Asset Management Guide - A Focus on Implementation*. 2013.
2. Dominguez, M.T., *Transportation Asset Management Plan*, N.Y.S.D.o. Transportation, Editor. 2019, New York State Department of Transportation: New York.
3. Moore, M., et al., *Reliability of visual inspection for highway bridges, volume I*. 2001, Turner-Fairbank Highway Research Center.
4. Agrawal, A.K., A. Kawaguchi, and Z. Chen, *Bridge element deterioration rates*. 2008, New York (State). Dept. of Transportation.
5. Morcous, G., *Developing deterioration models for Nebraska bridges.* 2011.
6. Agrawal, A.K., A. Kawaguchi, and Z. Chen, *Deterioration rates of typical bridge elements in New York.* Journal of Bridge Engineering, 2010. **15**(4): p. 419-429.
7. Val, D.V. and R.E. Melchers, *Reliability of deteriorating RC slab bridges.* Journal of structural engineering, 1997. **123**(12): p. 1638-1644.
8. Vu, K.A.T. and M.G. Stewart, *Structural reliability of concrete bridges including improved chloride-induced corrosion models.* Structural Safety, 2000. **22**(4): p. 313-333.
9. Wang, Y., et al., *Semi-empirical prediction model of chloride-induced corrosion rate in uncracked reinforced concrete exposed to a marine environment.* Electrochimica Acta, 2020. **331**: p. 135376.
10. Vidal, T., A. Castel, and R. Francois, *Analyzing crack width to predict corrosion in reinforced concrete.* Cement and concrete research, 2004. **34**(1): p. 165-174.

11. Stewart, M.G., *Spatial variability of pitting corrosion and its influence on structural fragility and reliability of RC beams in flexure.* Structural Safety, 2004. **26**(4): p. 453-470.

12. Bu, G., et al., *Development of an integrated method for probabilistic bridge-deterioration modeling.* Journal of Performance of Constructed Facilities, 2014. **28**(2): p. 330-340.

13. Wang, H., R. Ranade, and P. Okumus, *Seismic fragility of reinforced concrete bridge columns utilizing ductile fiber-reinforced concrete covers.* Structure and Infrastructure Engineering, 2021: p. 1-23.

14. Zhang, X., et al., *Corrosion-induced spalling of concrete cover and its effects on shear strength of RC beams.* Engineering Failure Analysis, 2021: p. 105538.

15. Moccia, F., M.F. Ruiz, and A. Muttoni, *Spalling of concrete cover induced by reinforcement.* Engineering Structures, 2021. **237**: p. 112188.

16. Su, R.K.L. and Y. Zhang, *A novel elastic-body-rotation model for concrete cover spalling caused by non-uniform corrosion of reinforcement.* Construction and Building Materials, 2019. **213**: p. 549-560.

17. Lu, C., W. Jin, and R. Liu, *Reinforcement corrosion-induced cover cracking and its time prediction for reinforced concrete structures.* Corrosion Science, 2011. **53**(4): p. 1337-1347.

18. Caré, S., et al., *Mechanical properties of the rust layer induced by impressed current method in reinforced mortar.* Cement and Concrete Research, 2008. **38**(8-9): p. 1079-1091.

19. Liu, Q. and R.K.L. Su, *A displacement-based inverse analysis method to estimate in-situ Young's modulus of steel rust in reinforced concrete.* Engineering Fracture Mechanics, 2018. **192**: p. 114-128.

20. Thomas, R., J. Eric Mann, and Z.M. Chill, *Bridge Inspector's Reference Manual*, U.S.D.o. Transportation, Editor. 2012, U.S. Department of Transportation: Washington, D.C.

21. AASHTO, *AASHTO Guide Manual for Bridge Element Inspection*. 2019.

22. NYSDOT, *Bridge Inspection Manual-NYSDOT*, NYSDOT, Editor. 2014, NYSDOT: New York State.

23. NYSDOT, *Bridge Inspection Manual*, N.Y.S.D.o. Transportation, Editor. 2017.

24. Veshosky, D., et al., *Comparative analysis of bridge superstructure deterioration.* Journal of Structural Engineering, 1994. **120**(7): p. 2123-2136.

25. Yanev, B. and X. Chen, *Life-cycle performance of New York City bridges.* Transportation Research Record, 1993. **1389**: p. 17.

26. Mauch, M. and S. Madanat, *Semiparametric hazard rate models of reinforced concrete bridge deck deterioration.* Journal of Infrastructure Systems, 2001. **7**(2): p. 49-57.

27. Weyers, R.E., et al., *Concrete Bridge Protection and Rehabilitation: Chemical and Physical Techniques. Service Life Estimates*. 1994.

28. Life-365™. *Life-365 service life predication model™*. 2020 [cited 2018 Sep. 9]; Available from: http://www.life-365.org.

29. Andrade, C. and C. Alonso, *On-site measurements of corrosion rate of reinforcements.* Construction and building materials, 2001. **15**(2-3): p. 141-145.

30. Cui, F., et al., *Seismic fragility analysis of deteriorating RC bridge substructures subject to marine chloride-induced corrosion.* Engineering Structures, 2018. **155**: p. 61-72.

31. El Maaddawy, T. and K. Soudki, *A model for prediction of time from corrosion initiation to corrosion cracking.* Cement and concrete composites, 2007. **29**(3): p. 168-175.

32. Yuan, Y., J. Jiang, and T. Peng, *Corrosion process of steel bar in concrete in full lifetime.* ACI Materials Journal, 2010. **107**(6): p. 562.

33. Otieno, M., H. Beushausen, and M. Alexander, *Chloride-induced corrosion of steel in cracked concrete–Part I: Experimental studies under accelerated and natural marine environments.* Cement and Concrete Research, 2016. **79**: p. 373-385.